Atmospheric Environment 94 (2014) 626–636

Contents lists available at ScienceDirect

Atmospheric Environment

journal homepage: www.elsevier.com/locate/atmosenv

Composition and hygroscopicity of aerosol particles at Mt. Lu in South China: Implications for acid precipitation

Weijun Li [a, *], Jianwei Chi [a], Zongbo Shi [b], Xinfeng Wang [a], Bin Chen [a], Yan Wang [c], Tao Li [c], Jianmin Chen [a, c, *], Daizhou Zhang [d], Zifa Wang [e], Chune Shi [f], Liangke Liu [g], Wenxing Wang [a]

[a] Environment Research Institute, Shandong University, Jinan, Shandong 250100, China
[b] School of Geography, Earth and Environmental Sciences, University of Birmingham, UK
[c] School of Environment Science and Engineering, Shandong University, Jinan, Shandong 250100, China
[d] Faculty of Environmental and Symbiotic Sciences, Prefectural University of Kumamoto, Kumamoto 862-8502, Japan
[e] State Key of Laboratory of Atmospheric Boundary Physics and Atmospheric Chemistry, Institute of Atmospheric Physics, Chinese Academy of Sciences, Beijing, 100029, China
[f] Anhui Institute of Meteorological Sciences, Anhui Institute of Meteorological Sciences, Hefei, 230031, China
[g] Nanjing University of Information Science and Technology, Jiangsu, 210044, China

HIGHLIGHTS

- SO_4^{2-} is the dominant ion in aerosol particles.
- Aerosol particles dominated by sulfate start to deliquesce at 63–76%.
- Large amounts of nano-sized metal particles embedded in 37% S-rich particles.
- SO_2 of long range transport from industries and fired-power plants in the YRD.

GRAPHICAL ABSTRACT

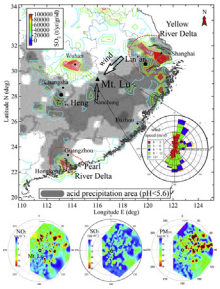

ARTICLE INFO

Article history:
Received 25 February 2014
Received in revised form
1 June 2014
Accepted 2 June 2014
Available online 4 June 2014

Keywords:
Acid precipitation
Hygroscopicity
Aerosol formation
Individual particle

ABSTRACT

Physicochemical properties of aerosol particles were studied at Mt. Lu, an elevated site (115°59′E, 29°35′N, 1165 m) within the acid precipitation area. Northeast winds transport copious amounts of air pollutants and water vapor from the Yangtze River Delta into this acid precipitation area. NH_4^+ and SO_4^{2-} are the dominant ions in $PM_{2.5}$ and determine aerosol acidity. Individual particle analysis shows abundant S-rich and metals (i.e. Fe-, Zn-, Mn-, and Pb-rich) particles. Unlike aerosol particles in North China and urban areas, there are little soot and mineral particles at Mt. Lu. Lack of mineral particles contributed to the higher acidity in precipitation in the research area. Nano-sized spherical metal particles were observed to be embedded in 37% of S-rich particles. These metal particles were likely originated from heavy industries and fired-power plants. Hygroscopic experiments show that most particles start to deliquesce at 73–76% but organic coating lowers the particle deliquescence relative humidity (DRH) to 63–73%. The DRHs of these aerosol particles are clearly smaller than that of pure ammonium sulfate particles which is 80%. Since RH in ambient air was relatively high, ranging from 65% to 85% during our study period, most particles at our sampling site were in liquid phase. Our results suggest that liquid

* Corresponding authors. Environment Research Institute, Shandong University, Jinan, Shandong 250100, China.
E-mail addresses: liweijun@sdu.edu.cn (W. Li), jmchen@sdu.edu.cn (J. Chen).

http://dx.doi.org/10.1016/j.atmosenv.2014.06.003

phase reactions in aerosol particles may contribute to SO_2 to sulfuric acid conversion in the acid precipitation area.

1. Introduction

Airborne pollutants are deposited on the earth's surface by 1) wet deposition (rain and snow); 2) dry deposition (particles and gases). Acting as condensation cloud nuclei (CCN) and ice nuclei (IN), aerosol particles influence the climate system indirectly by altering cloud microphysics and albedo (IPCC, 2007), hydrological balance (Ramanathan et al., 2001), and the ecosystem (Bormann, 1985). In the past two decades, rapid industrialization and urbanization in China have contributed large quantities of anthropogenic pollutants into the atmosphere.

Recently, research activities in China have been directed to understand the formation of haze-fog events in East China, with the Chinese government starting to improve air quality in the megacities (Zhang et al., 2012). On the other hand, acid precipitation has been to some extent overlooked, even though it covers 12.9% of the continental area of China (AEAERC, 2011). The world's third largest acid rain area has emerged in this region in the past thirty years, following Europe and North America (Galloway et al., 1987; Wang and Wang, 1995; Li et al., 2010b; Tang et al., 2010). The impact of anthropogenic air pollutants on precipitation composition and the subsequent effects on aquatic and terrestrial ecosystems have been well recognized in North America, Scandinavia, South China, and Europe over the past decade (Bormann, 1985; Galloway et al., 1987). Progress report from the U.S. Environmental Protection Agency (EPA, 2006) showed that the developed countries in past decades that have pursued the tenets of the Clean Air Act have substantially reduced the size of the acid precipitation area. Conversely, in South China the acid precipitation area increased slightly and has been shown to occur throughout this period (Tang et al., 2010).

The largest, contiguous acid-impacted region is south of the Yangtze River, according to the AEAERC in 2011. Tang et al. (2010) suggest that the center of the severe acid rain area south of the Yangtze River moved eastwards to include Jiangxi and Zhejiang provinces. In the acidic cloud water or rain water of south China, SO_4^{2-} dominates followed by NH_4^+, NO_3^-, Ca^{2+}, Cl^-, F^-, K^+, Na^+, and Mg^{2+} (Lei et al., 1997; Cao et al., 2009; Huang et al., 2009, 2010; Li et al., 2010b; Sun et al., 2010). Recently, Li et al. (2013b) showed that strongly acidic clouds (pH, ~3.5) cover Jiangxi province and form acid rain in summer. The study further suggested that the acidic cloud droplets enhance the soluble efficiency of nano-sized metals in clouds, which may lead to additional adverse impacts on the ecosystem and human health in South China.

Once aerosol particles act as CCN, chemical properties of individual aerosol particles can affect the acidity of the corresponding cloud droplet, thereby pointing out the importance of understanding the physicochemical properties of aerosol particles in the acid precipitation area. In particular, the chemical composition of aerosols among various size ranges is a key factor in determining their hygroscopicity, CCN activity, and optical properties (Hudson, 2007). Individual aerosol particles are a complex mixture of inorganic and organic species, and soluble and insoluble species contributed directly or indirectly by anthropogenic and natural sources (Li and Shao, 2009; Posfai and Buseck, 2010). When considering the influence of aerosol particles in one region, one first needs to understand their chemical composition and mixing state (Hudson, 2007; Twohy and Anderson, 2008; Posfai and Buseck, 2010; Adachi et al., 2011; Li et al., 2011a). Individual particle analysis by transmission electron microscopy (TEM) has become a reliable technique to characterize aerosol particles which range in size from nanometer to micrometer, as well as provide information on their sources, morphology, and mixing state (Li and Shao, 2009).

Hygroscopic characterization of aerosol particles has important implications for their environmental effects (Martin, 2000; Wise et al., 2009; Freney et al., 2010; Peckhaus et al., 2012). If aerosol particles contain highly hygroscopic species such as sulfates, nitrates, or soluble organic acids, they would take up water when the relative humidity (RH) is high enough and grow into cloud droplets at certain supersaturation conditions (Martin, 2000; Hudson, 2007). Water absorbing hygroscopic components can change both diameter and wavelength dependent refractive indices of individual particles (Lack et al., 2009; Adachi et al., 2011). Therefore, it is necessary to quantify the hygroscopicity of aerosol particles in acid precipitation areas with high RH.

The objective of this paper is to characterize the chemical composition and hygroscopicity of individual aerosol particles in an acid deposition area in South China. In this study, aerosol samples were collected near the summit of Mt. Lu (115°59′E, 29°35′N, 1165 m) in Jiangxi province, the center of the heavy acid precipitation area in South China. Chemical composition and mixing state of individual particles were investigated using transmission electron microscopy (TEM). We also studied the hygroscopicity of individual particles using a newly developed individual particle hygroscopic (IPH) system.

2. Experiments

2.1. Sampling site

Mt. Lu, covering an area of 300 km^2 (115°59′E, 29°35′N, 1165 m), is located south of Jiujiang city in northern Jiangxi Province, China, between the Yangtze River and Boyang Lake. Mt. Lu is 700 km northwest of the Pearl River Delta (PRD) and 400 km southwest of the Yangtze River Delta (YRD) (Fig. 1). Mt. Lu lies within the Asian humid continental and tropical monsoon climate zone, where cloud/fog and rain events are common from spring to autumn. Fig. 1 shows that the Mt. Lu area is located within the acid precipitation area of South China. The town of Guling on top of Mt. Lu has a population of about 10,000; most residents work in tourism or related services, so relatively little local pollution is produced. There are some large steel and oil refining industries and coal-fired power plants in the YRD and non-ferrous mines associated with non-ferrous mining, smelting, and refining of pure metals in Jiangxi province. Therefore, the major SO_2 emission sources are located in the YRD but outside of Shanghai city.

2.2. Meteorology

The dominant wind direction below 1500 m during the summer season in South China is from the Northeast, which brings water vapor and pollutants into acid precipitation area (Figs. S1–S4 in Supporting Information (SI)). The sampling was conducted during 11 August to 23 September, 2013. The average temperature and relative humidity (RH) were 23 °C and 80% during non-cloud periods, respectively. Thirty 48-h air mass back trajectories ending at Mt. Lu from 14 to 24 November were simulated by HYSPLIT model

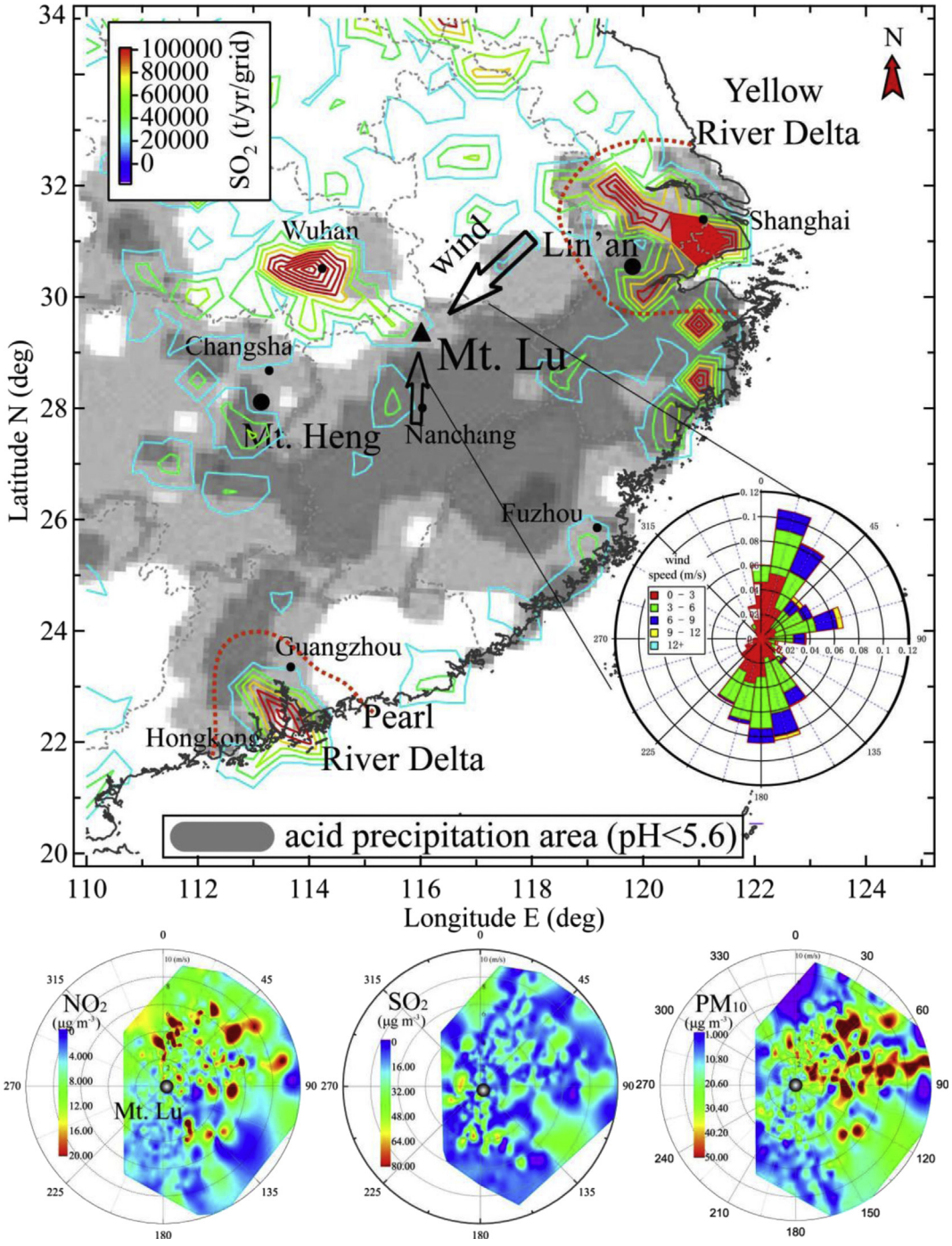

Fig. 1. The location of Mt. Lu (115°59′E, 29°35′N, 1165 m) in the acid precipitation area wind rose, and concentration distribution for PM_{10}, SO_2, and NO_2 associated with wind speed and directions from 1 August to 26 September, 2011. Mt. Heng (27.3° N, 112.7° E, elevation at 1269 m) as one elevated site and Lin'an station (30.3° N, 119.7° E) as one regional background site, are marked in the acid precipitation area. The data of acid precipitation area were obtained from the Annual Environment Report of China in 2011 and the contours represent the SO_2 emission distributions in East China (units: t/year/grid, grid size: 0.5°, data from Zhang et al. (2009)).

(http://ready.arl.noaa.gov/HYSPLIT.php) (Fig. S2). Most of air mass back trajectories were from South and Northeast areas of Mt. Lu in South China.

2.3. Aerosol sampling and analysis

Aerosol particles were collected on copper TEM grids coated with carbon film (carbon type-B, 300-mesh copper, Tianld Co., China) by a single-stage cascade impactor with a 0.5-mm-diameter jet nozzle and an air flow rate of 0.5 l min^{-1}. For these conditions, the calculated size (d_{50}) is ~0.5 μm (Marple et al., 1993). Because the air quality has small changes at Mt. Lu, each sampling time was set up at 4 min in non-cloud periods. Clouds or fog frequently occurred during our sampling period. After sample collection, we immediately used optical microscopy with magnification from ×500 to ×1200 to check whether the carbon film and aerosol distribution on the TEM grids were suitable for analysis. Then, the grid was placed in a sealed, dry plastic tube and stored in a desiccator at

25 °C and 20 ± 3% RH to minimize exposure to ambient air and preserve it for analysis. Finally, nine samples collected in clear periods during 14 August–23 September, 2013 were selected and analyzed by TEM.

Aerosol particles on the TEM grids were analyzed with a JEM-2100 TEM operated at 200 kV. Particles examined by TEM were dry at the time of observation in the vacuum of the electron microscope. The effects of water, semi-volatile organics, and NH_4NO_3 could not be considered. Elemental composition was determined semi-quantitatively by an energy-dispersive X-ray spectrometer (EDS) that can detect elements heavier than carbon. EDS spectra were collected for only 15 s to minimize radiation exposure and potential beam damage. Copper could not be analyzed because of interferences from the copper TEM grid. EDS data obtained from INCA software under channel 4–5. In this study, TEM images with magnification between ×2000 and ×5000 were quickly obtained from the center to the periphery of each sample. The procedure ensured that the aerosol distribution and morphology over the entire sample was obtained. To understand the morphology, composition, size, and mixing state of each aerosol particle, TEM images were taken and EDS was used to determine the composition of their component parts such as coatings, inclusions, and aggregates. In order to understand elemental distributions in individual aerosol particles, the elemental mapping experiments were conducted by the JEM-2100F TEM with a scanning TEM (STEM) function. Equivalent circle diameter in two dimensions was determined using the iTEM software (Olympus soft imaging solutions GmbH, Germany) (Li et al., 2013a).

A MiniVol sampler (Airmetrics, USA) with a constant pumping rate of 5 l min^{-1} was employed to collect $PM_{2.5}$ on quartz-fiber filters for the analysis of soluble inorganics. Thirty $PM_{2.5}$ samples and two blank samples as the reference filters were collected in non-cloud periods from 11 August to 23 September, 2011. The sampling periods ranged from 4 h to 23.5 h depending on the cloudy and rainy periods in different days. In addition, we collected the cloud water during cloud or fog periods and cloud water was acidic, with a pH of 3.52 at Mt. Lu. The detailed information about cloud water can be found in Li et al. (2013b). The $PM_{2.5}$ samples were stored at refrigerator at Mt. Lu and were put in one icebox during the transportation from sampling site to our laboratory, which kept the temperature lower than 0 °C. Five cations (Na^+, K^+, NH_4^+, Ca^{2+}, and Mg^{2+}) and five anions (F^-, Cl^-, NO_2^-, NO_3^-, and SO_4^{2-}) were quantified by ion chromatography (IC). Because of limitation from the IC detection, we only obtained concentration of nine ions (see Section 3.2). The hourly mass concentrations of SO_2, NO_2, and PM_{10} were provided by an automatic environmental monitoring station, about 5 m from the sampling site. In this study, we obtained valid concentration data of PM_{10} ($n = 1112$ h), SO_2 (972 h), and NO_2 (493 h) (Fig. 1). Wind speed, wind direction, relative humidity (RH), barometric pressure, and ambient temperature were obtained from the local meteorological station. In this study, the wind vector maps in different altitudes in South China are shown in supplemental material (Figs. S3 and S4).

2.4. Hygroscopic experiments of individual aerosol particles

One individual particle hygroscopic (IPH) system was built for observing hygroscopic properties of individual particles at different relative humidities. The measurement system consisted of three steps: (1) Introducing wet and dry N_2 gas with controlled flow into one chamber, controlled by two mass control flow meters. (2) Setting the TEM grids with aerosols on the bottom of one stainless steel column chamber (size: 20 mm (height) × 30 mm (diameter)) with two holes on top and bottom side covered by two microscope slides. RH and temperature sensors of a digital hygrometer (Testo 645, ±1%) were inserted into the chamber from its side. (3) Obtaining images in different relative humidity through one inverted microscope (IBE2003, China) with a camera (Canon 650D). NaCl aerosols were generated from 1 M solutions. We used the same procedure from Wise et al. (2005) to make the standard samples in the laboratory. Laboratory-generated NaCl particles on TEM grids were used to calibrate the system (Fig. S5). Detailed descriptions of the similar measurement system were given by Ahn et al. (2010). Similar IPH systems have successfully observed hygroscopic growth observations of field-collected and laboratory-generated aerosols with the diameter larger than 0.5 μm (Ahn et al., 2010; Peckhaus et al., 2012; You et al., 2012). Here two samples of particles with organic coating and particles with non-coating were chosen to observe particle hygroscopic growth. The IPH system observed the particle deliquescence and efflorescence at the RH range from 3% to 90% under one stable room temperature at 20 °C.

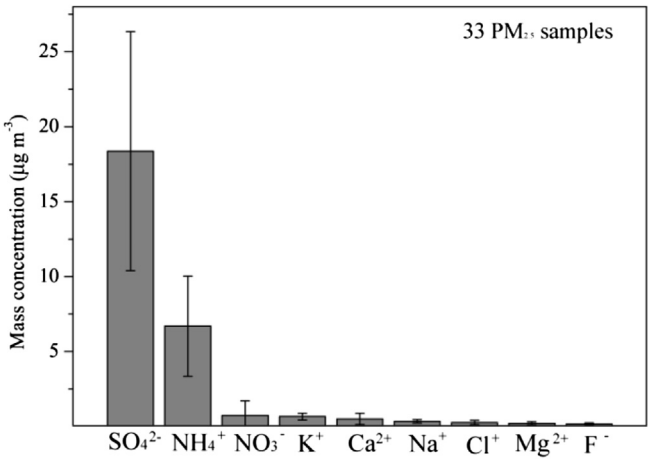

Fig. 2. Average soluble inorganic ions concentration in 33 $PM_{2.5}$ samples at Mt. Lu in summer.

3. Results and discussion

3.1. Transport of gas and aerosol pollutants

Wind direction and wind speed are the most important factors for transport of air pollutants in the troposphere. Examining wind direction, wind speed, and pollutants at Mt. Lu, Fig. 1 shows two major transport paths: from the northeast and from the south. Fig. S3 shows that mean wind in August and September is from the northeast. These results were consistent with 48-h air mass back trajectories as shown in Fig. S2. The northeasterly wind apparently brought air pollutants and water vapor from the coastal YRD into the acid precipitation area. 42% (by hour) PM_{10} data, 46% SO_2, and 42% NO_2 occur with northeast winds, with their average hourly concentrations at 28 μg m^{-3}, 16 μg m^{-3}, and 11 μg m^{-3}, respectively (Fig. 1). Wind rose data (bottom of Fig. 1) also showed a possible source of PM_{10} from the northeast direction, that is, the YRD. The southerly wind possibly brought air pollutants from Jiangxi province. 37% PM_{10} data, 31% SO_2, and 37% NO_2 occur from northeast winds, with their average hourly concentrations at 15 μg m^{-3}, 17 μg m^{-3}, and 5 μg m^{-3}, respectively. Fig. 1 also shows that the SO_2 emission sources, including heavy industries and coal-fired power plants, lie within the YRD, indicating that air pollutants from the northeast could have contributed to the air pollution on Mt. Lu. The SO_2 wind rose data did not show any particular emission source in the major wind directions. The reason can be attributed to its relatively short lifetime of SO_2 or the region emission sources.

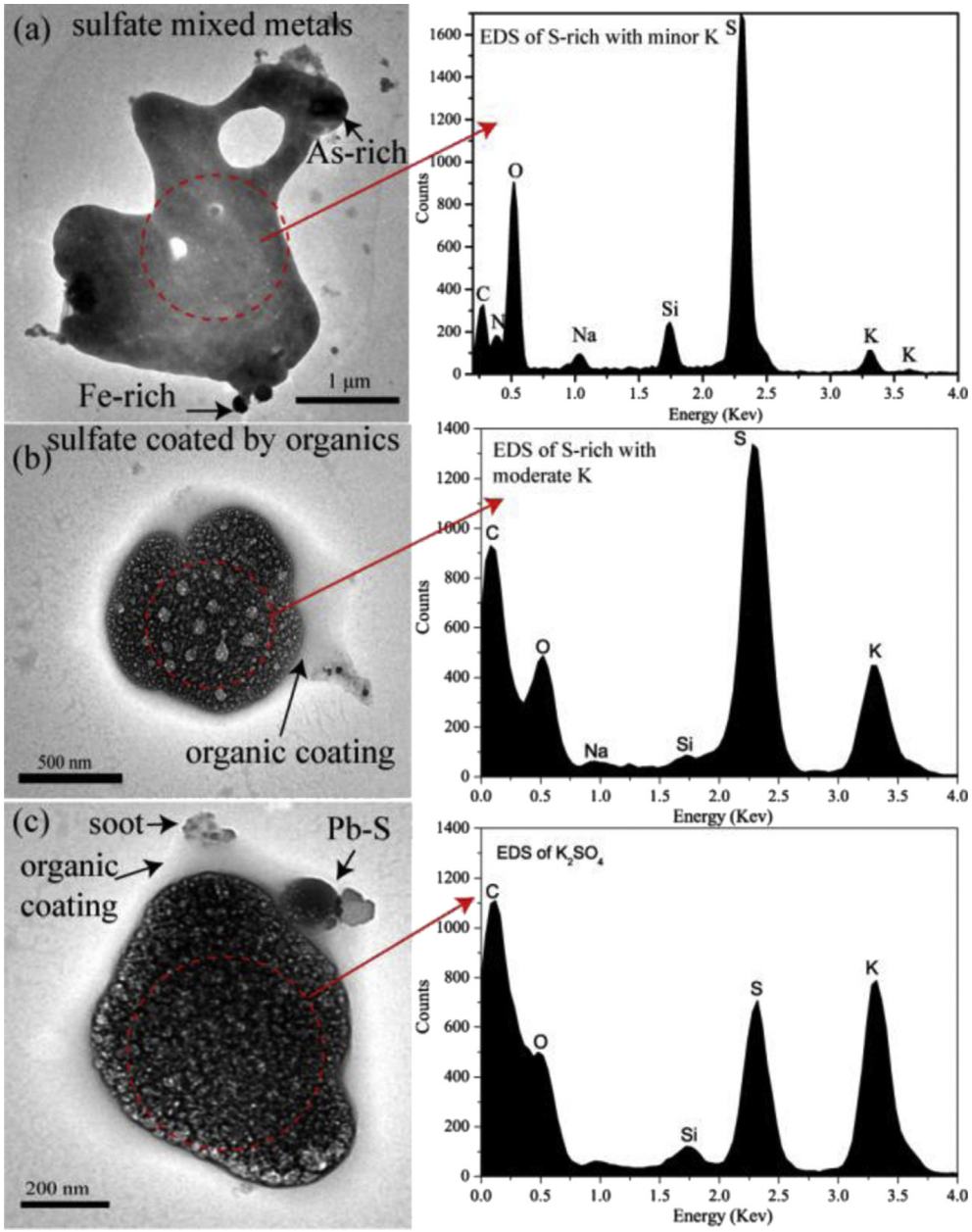

Fig. 3. Three different types of individual S-rich particles. (a) S-rich particle with minor K mixed with one As-rich particle and one Fe-rich particle. EDS data obtained from INCA software under channel 5. (b) S-rich particle with moderate K coated by organics. (c) K_2SO_4 particle mixed with organic coating, soot, and Pb–S. EDS data obtained from INCA software under channel 4.

3.2. Soluble inorganic ions in $PM_{2.5}$

Nine inorganic ions were quantified in 35 $PM_{2.5}$ samples. Fig. 2 shows that the highest inorganic ion is SO_4^{2-} with a concentration of 18.4 ± 8.0 μg m^{-3}, close to the 17.2 μg m^{-3} at the regional background station of Lin'an and more than two times higher than that at Mt. Heng in Hunan province (Xu et al., 2002; Gao et al., 2012). Sun et al. (2010) showed that SO_4^{2-} was the dominant anion, followed by NO_3^-, both of which control the acidity of cloud water at Mt. Huang in spring.

Interestingly, the mass concentration of NO_3^- at 0.71 ± 0.99 μg m^{-3} is lower than 1.5 μg m^{-3} at Mt. Heng (Gao et al., 2012). The partition of NO_3^- between the gas and particulate phases strongly depends on temperature, with lower temperatures favoring the partition of ammonium nitrate in the particulate phase. Indeed, air temperatures ranging from 19 °C to 29 °C at Mt. Lu in this study are much higher than the springtime temperatures at Mt. Heng (9.8 °C–16.3 °C). Fig. 2 shows that NH_4^+ at 6.68 ± 3.3 μg m^{-3} is the major cation to neutralize acidic components. Additionally, K^+ concentration at 0.65 ± 0.22 μg m^{-3} at Mt. Lu is higher than 0.43 μg m^{-3} at Mt. Heng reported by Gao et al. (2012), who suggested that biomass burning contributed potassium salts in the atmosphere over the precipitation area. The average cation/anion (C/A) ratio is 0.94 in $PM_{2.5}$ samples, suggesting that ammonium sulfate could be the dominant component in the $PM_{2.5}$.

Soluble ions of 54 cloud water samples show that SO_4^{2-} dominated 30% of the total ions in cloud water, following by NH_4^+ (24%) at

Mt. Lu during this period (Yang, 2013). Therefore, SO_4^{2-} is the dominant acidic ion in both aerosol particles and cloud droplets and contribute to the acidity of cloud water and rain at Mt. Lu in summer.

3.3. Main individual particle types

Based on elemental composition and morphology of individual particles, we identified six different particle types: S-rich, metal (including fly ash), organic matter, soot, K-rich, and mineral. S-rich particles were a dominant aerosol type in all size ranges, which are internally mixed with metal, organic matter, soot, K-rich, and mineral (Fig. S6). The result is consistent with the SO_4^{2-} as the dominant ion in $PM_{2.5}$. In the internally mixed particles, various metal particles were embedded within individual S-rich particles, and secondary organic matter coated onto the surface of S-rich particles, as shown in Figs. S6 and 3. These observations are consistent with previous studies (Li et al., 2013b) where large amounts of nano-sized metal particles were measured in the atmosphere at Mt. Lu.

3.3.1. Sulfates

S-rich particles contained S and O, with certain amounts of K, Na, C, and N (Fig. 3a). S-rich particles at Mt. Lu could be mainly composed of $(NH_4)_2SO_4$ and minor $(NH_4)HSO_4$, organic matter, and K_2SO_4. Although TEM analysis cannot give nitrate information, NH_4NO_3 cannot be excluded in this study according to the soluble ions in $PM_{2.5}$ shown in Fig. 2. Many studies already show that individual secondary particles commonly contain ammonium sulfate and ammonium nitrate in the atmosphere (Whiteaker et al., 2002; Middlebrook et al., 2011; Hao et al., 2013). As a result, we can speculate that individual secondary particles could mainly contain sulfates with other minor particle species.

The second dominant type of S-rich particles contains certain amounts of K (Fig. 3b). The fraction of K in S-rich particles is lower than K_2SO_4 in Fig. 3c. We suggests that certain amounts of potassium salts coexisted in secondary sulfate particles, which has been commonly observed in cloud droplets at Mt. Lu (Li et al., 2013b). TEM analysis revealed that this kind of S-rich particle significantly contributed soluble K^+ to $PM_{2.5}$ shown in Fig. 2. We also found that the S-rich particles were coated frequently by organic matter. Li et al. (2010a) observed similar particles in Beijing air influenced by agricultural biomass burning. In the present study, only small numbers of K_2SO_4 particles were shown in Fig. 3b and abundant S-rich particles with minor K were founds at Mt. Lu. Here we can presume that particles (e.g., KCl and K_2SO_4) from biomass burning can transform into S-rich particles with certain amounts of K through processing in cloud droplets or condensations of SO_2 and H_2SO_4.

3.3.2. Metal particles

Numerous metal particles occurred at Mt. Lu and were internally mixed with S-rich particles (Fig. 4). One low-magnification TEM image displays ten S-rich particles, six of which include metal inclusions confirmed by EDS. Many metal particles look like an aggregation of several metal particles. Since small sized metal particles have a higher density, they are darker than other aerosol particle types and are therefore easy to be identified. For example, Fig. 5 shows two dark dots in the S-rich particle and their composition reveals two metal particles (Fe-rich and Pb-rich). Li et al. (2013b) found four major metal types at Mt. Lu in cloud droplets: Pb-rich (35%), fly ash including minor metals (27%), Fe-rich (23%), and Zn-rich (15%). We still found that Pb, Fe, and Zn in metal particles were the dominant elements in aerosol particles. These metal particles exhibit a nearly spherical shape (e.g., Fig. 5), suggesting that they likely come from industrial processes and coal-fired power generation via high-temperature combustion followed by fast cooling (Giere et al., 2006). There are various large steel and oil refining industries and coal-fired power plants in YRD and many non-ferrous smelting industries are distributed throughout Jiangxi province.

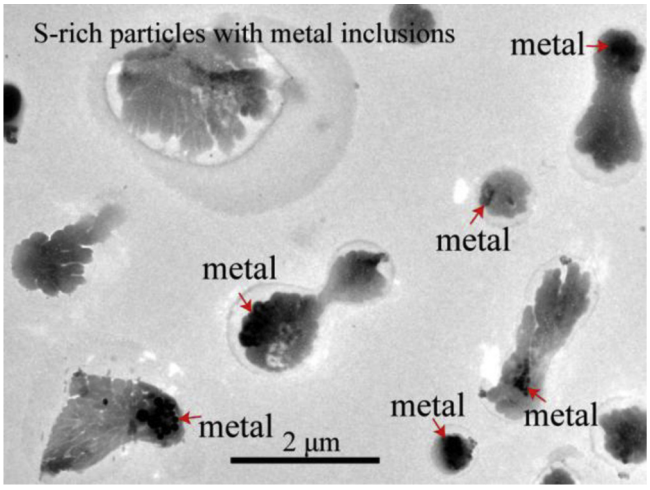

Fig. 4. One low-magnification TEM image showing metal inclusions in S-rich.

Li et al. (2013b) show that acidic cloud droplets can dissolve nano-sized metal particles into sulfates. We carefully examined the composition of individual metal-bearing particles. In this study, we found that 37% of S-rich particles had metal inclusions. For example, Fig. 6 shows the Sn–O and Pb–S particles were internally mixed with S-rich particles. Once this kind of aerosol particles act as CCN, SO_2 oxidation catalyzed by metal ions could be the dominant in-cloud oxidation pathway (Harris et al., 2013).

3.3.3. Soot and mineral particles

Many studies showed that soot and mineral particles were the major particle types in the atmosphere and were commonly found in aerosol samples collected at mountain site and ground level (Li and Shao, 2009; Posfai and Buseck, 2010; Li et al., 2011b). TEM analysis display a rather low number of soot and mineral particles at Mt. Lu (Fig. 7). The typical soot particles in Fig. S6g were difficult to be found at Mt. Lu and some tiny soot particles were internally mixed with organic or sulfate (Fig. 3c). A few elongate regular $CaSO_4$ were detected in the samples but the $Ca(NO_3)_2$ coated on mineral particles occurring at Mt. Tai and urban cities in North China (Li and Shao, 2009) had been not found at Mt. Lu. In addition, some mineral particles mixed with metal particles as shown in Figure S6e occurred in fine and coarse particles. Such mixed mineral particles were considered as the emissions of industries and fired-power plant instead of natural soil.

3.3.4. Organic matter

Most organic matter was internally mixed with secondary particles at Mt. Lu. Most organic aerosols can not be clearly identified in secondary particles (Fig. 3a) although some can be identified as the organic coatings (Fig. 3b–c). Therefore, we classified the internally mixed particles of organic and sulfate in Fig. 3b as S-rich particle type. Only small number of particles in the samples at Mt. Lu were dominated by organic matter, as shown in Fig. S4a.

3.4. Size and mixing of different particle types

Fig. 7 shows the relative abundance of 1634 particles from 80 nm to 4 μm. The S-rich particles account for 82% of all analyzed

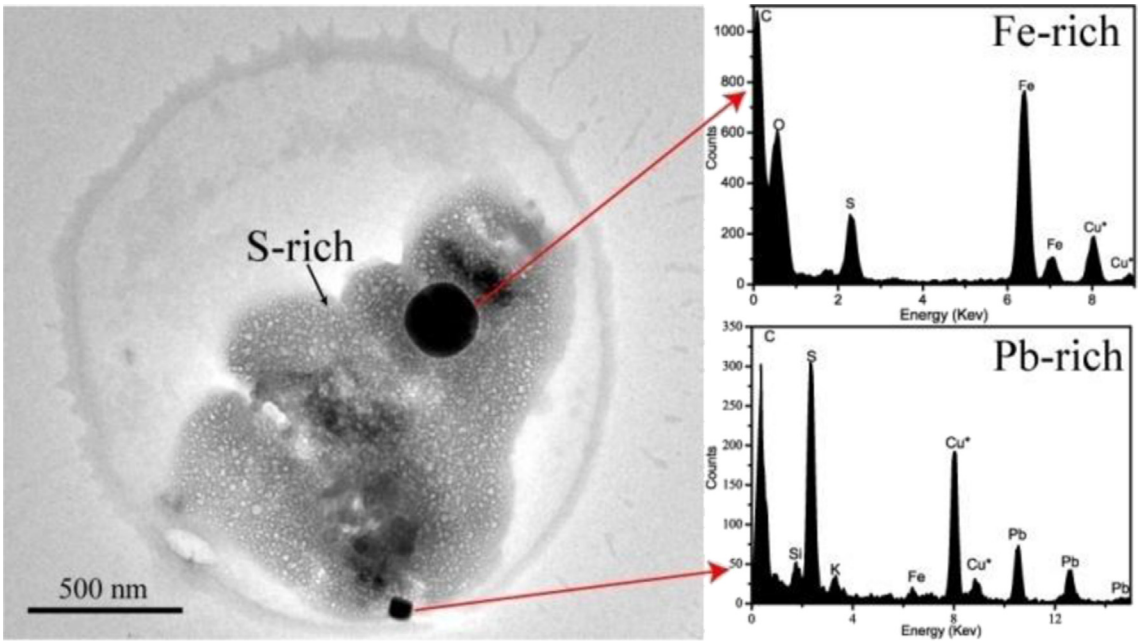

Fig. 5. TEM image and EDS of two metal inclusions in one S-rich particle.

particles and are the dominant particle type in all size bins. 46% of 1388 analyzed S-rich particles were defined as internally mixed particles that include fly ash, metal, soot, or mineral, except for the organic matter that cannot be clearly identified (Fig. 5). Although 18% particles were not classified as S-rich particles, they still contained certain amounts of sulfates. In all, morphology, composition, and mixing state of individual particles at Mt. Lu in South China were more homogeneous than those at Mt. Tai (1535 m) in North China (Li et al., 2011b). In addition, only 6% of S-rich particles contained soot inclusions at Mt. Lu are much lower than at Mt. Tai in North China where 72%–83% of S-rich particles included soot inclusions (Li et al., 2011b). The low percentage of soot and mineral particles at Mt. Lu differs from the aerosol distribution in North China where soot and mineral particles were dominant in sizes smaller than 1 μm and larger than 2 μm (Li and Shao, 2009; Li et al., 2011b). In addition, 6% and 3% of 1388 S-rich particles mixed soot and mineral particles.

3.5. Hygroscopic properties of individual particles

Hygroscopic properties of individual particles from two different samples exhibit different hygroscopic growth factors. Fig. 8a shows that particles collected on 4 September begin to grow at 73–76% with the average grow factor (GF) at 1.006 and that dramatic growth occurs at 80% with the average GR at 1.13. Fig. 8b shows that particles collected on 5 September begin to grow at 63–73% with the average GR at 1.04 but that part of them display dramatic growth at 80% with the average GR at 1.23. The dramatic changes of growth factor at 80% suggest that these secondary particles completely transformed from solid phase to liquid phase in two samples. When the humidity increase 90%, the GR values increase the largest at 1.26 in Figs. 8a and 1.38 in Fig. 8b. Additionally, the particles in these two samples have similar dehydration curves with the efflorescence RH (ERH) at 49–53%. Although the particles in the two samples have similar DRH and ERH, they exhibit different hygroscopic growth trends.

A number of studies have shown that hygroscopic properties of aerosol particles are dependent on their chemical composition (Martin, 2000; Choi and Chan, 2002; Shi et al., 2012). Fig. 2 shows that SO_4^{2-} is the dominant ion in fine particles, consistent with the dominant S-rich particles found in individual particle analysis. Individual ambient particles normally start to deliquesce at lower RH than the DRH at 80% of the pure $(NH_4)_2SO_4$. This result can be attributable to the mixtures of two or more inorganic species (e.g., $(NH_4)_2SO_4$, $(NH_4)HSO_4$, K_2SO_4, or NH_4NO_3) within the same individual particles (discussed in section 3.3.1) (Freney et al., 2009). In particular, particles shown in Fig. 8b start to deliquesce at 63–73% – much lower than those at 73–76% shown in Fig. 8a. The ion analysis and TEM observations together showed similar inorganic ions and particle types, but TEM images revealed thin organic layers coated on some particles in Fig. 8b. Soluble organic species in the internally mixed particles may cause the water absorption of organic materials at low RH than inorganic materials (Varutbangkul et al., 2006) and change the hygroscopic growth of aerosol particles (Brooks et al., 2002; Choi and Chan, 2002). Therefore, the soluble organic coatings probably induce the early deliquescence of individual particles. Shi et al. (2012) showed that the internally mixed $(NH_4)_2SO_4$-benzoic acid particles display deliquescence earlier than the DRH of pure $(NH_4)_2SO_4$ particles. Also, the ratio of organic and inorganic ions in individual particles determines their deliquescent transitions (Peckhaus et al., 2012). These results suggest that soluble organic coatings and mixtures of multi-inorganic species account for the lower DRH of individual particles at Mt. Lu compared to that of ammonium sulfate.

The ambient RH during the sampling periods ranged from 65% to 85%. Based on the hygroscopic experiments, we conclude that the some or all the aerosol particles in non-cloud periods suspended as the liquid phase or liquid–solid phase while suspended in air. Therefore, the liquid water around the deliquesced particles provide an important media for gaseous SO_2 to sulfate conversion.

3.6. Implications of acid precipitation

Heavy acid precipitation in South China mostly occurs in highland areas with altitudes of 500–1500 m, where SO_2 emissions are low (Fig. S3). Fig. 1 shows the largest and highest intense SO_2

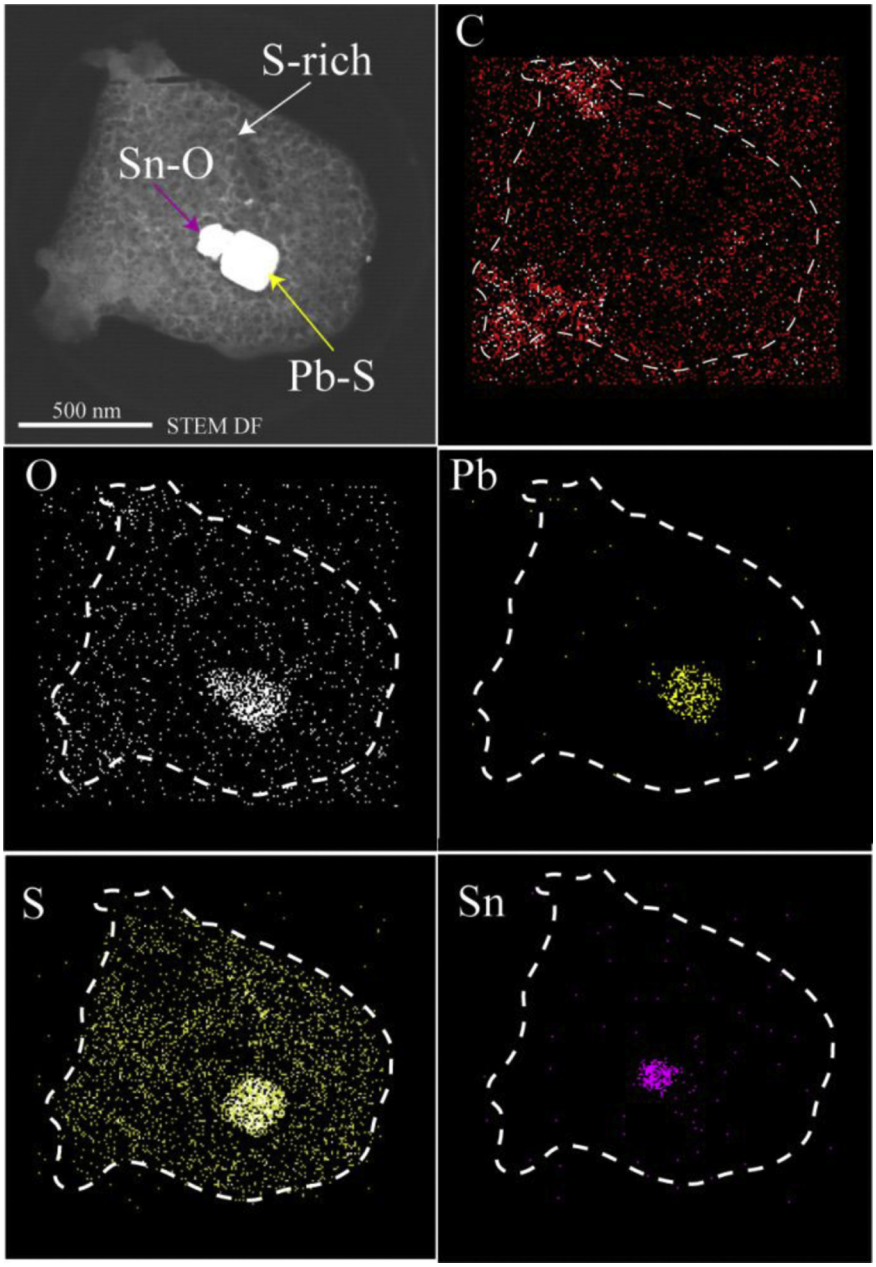

Fig. 6. Elemental mapping of an individual metal-bearing particle obtained from the STEM. A dark-field TEM image of the individual particle and each elemental distribution are shown.

emissions in South China in the YRD, one area that is upwind of Mt. Lu in summer. The dominant wind is from the east during sampling periods; therefore, the SO_2 emissions could be readily transported into the acid precipitation area and be transformed into secondary sulfates. Large amounts of secondary particles dominated by SO_4^{2-} can be formed during long-range transport and can further be CCN in acid clouds. Based on the composition and hygroscopicity of aerosols in the present study and results from Harris et al. (2013), we summarized the SO_2 oxidation during long-range transport in Figure S7a. Liquid layer formation on secondary particles due to early deliquescence probably enhance SO_2 oxidation through heterogeneous reactions in multiphase environment (Ravishankara, 1997).

Compared to small amounts of mineral and soot particles from ground-level sources such as road dust, ground soil, and vehicle emissions, the abundant metal particles at Mt. Lu suggest that the large amounts of gaseous and particulate emissions from major industries and power plants can reach high altitudes. As a result, transition metals from anthropogenic sources could catalyze SO_2 oxidation in clouds (Harris et al., 2013). In addition, the low concentrations of Ca^{2+} and Mg^{2+} in $PM_{2.5}$ and rather low number of mineral particles from TEM analysis both suggest that the alkaline mineral particles have limited acidic buffering capacity at Mt. Lu. Therefore, absence of mineral particles in the air likely contributes to the higher acidity of aerosol particles. These phenomenon indicated above can be attributed to the seasonal meteorological situation in South China and the height of emission sources – both critical for determining the transport distance (Kahn et al., 2008; Chen et al., 2013). Firstly, the humid air and frequent rains limit vertical transport of ground-level urban pollutants such as soil dust

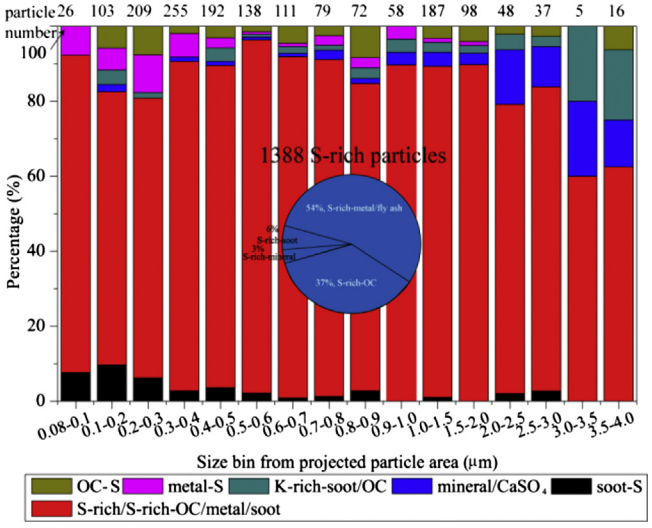

Fig. 7. Proportions of aerosol particles collected at Mt. Lu during 11 August to 23 September, 2011 in acid precipitation area. A total of 1634 aerosol particles were identified by their different morphology and composition. The number of the analyzed aerosol particles in different size ranges is shown above each column.

and vehicle emissions raise up to planetary boundary layer. Secondly, the large industries and power plants with their tall stacks can emit air pollutants into higher atmospheric levels (Chen et al., 2013). Fig. S4 shows that wind speed is at 3–10 m/s at 1000 m and <3 m/s on the ground during the sampling period. Therefore, the pollutants at high altitude can be dispersed quickly and transported for long distance. In addition, biomass burning plumes can reach the free troposphere because their buoyancy can be sufficient to lift smoke above the near-surface boundary layer (Kahn et al., 2008).

Based on our results and discussion, we devised one conceptual model that describes air pollutant emissions and their transport in Figure S7b. Massive amounts of air pollutants (e.g., SO_2 and metal) from coal-fired plants, heavy industries, and biomass burning are readily transported into upper levels of the troposphere. The summer monsoons likely drive large amounts SO_2 and water vapor from east lowland areas to west highland areas in South China. Therefore, beside pollutants' emission and transport, regional meteorological properties (i.e. wind and humidity) and terrain also significantly affect acidic cloud formation.

4. Conclusions

Soluble inorganic ions and individual aerosol particles were studied in summer at Mt. Lu. Northeast winds transported air pollutants from the YRD into the acid precipitation area, with the average hourly concentrations at 28 μg m^{-3} for PM_{10}, 16 μg m^{-3} SO_2, and 11 μg m^{-3} for NO_2. SO_4^{2-} is the dominant acidic ion in aerosol particles and could determine the acidity of cloud water and rain at Mt. Lu. In addition, absence of mineral particles in the air lead to their limited acidic buffering capacity and conversely aerosol particles become more acidic at Mt. Lu.

The secondary particles occurred in all sizes and S-rich particles were the dominant particle type, accounting for 82% of all analyzed particles. The study indicates that individual particles contain multi-inorganic species with the major compound being $(NH_4)_2SO_4$ with lesser amounts of NH_4HSO_4, NH_4NO_3, or K_2SO_4. The hygroscopic experiments show that individual particles start to deliquesce at 73–76%, although the secondary particles completely deliquesce at 80%. In addition, the soluble organic coatings on secondary particles can start deliquescence at 63–73% of individual particles but still completely deliquesce at 80%. Considering the ambient RH of 65–85%, the secondary particles should be in the liquid phase or liquid–solid multiphase in air. We found large

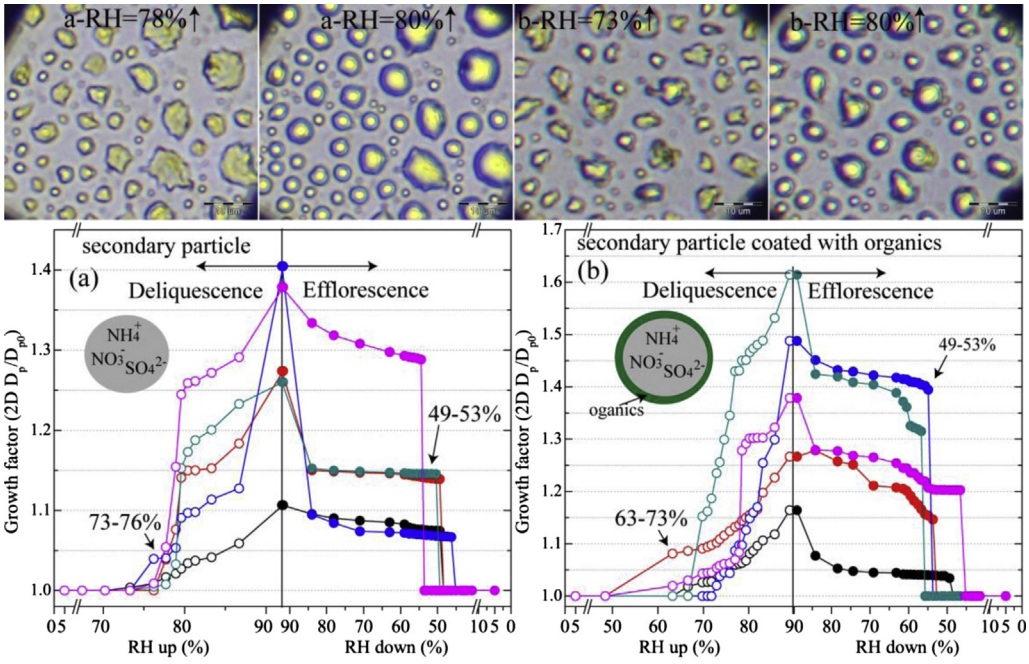

Fig. 8. Deliquescence and efflorescence of each particle with one color from 3% to 90% RH. (a) the sample collected on 4 September, 2011 containing secondary particles (b) the sample collected on 5 September, 2011 containing secondary particles with organic coating. Compositions of individual particles in the two samples were examined by TEM/EDS as shown in Fig. S6. Mixing state and composition of individual particles were described in the scheme. (For interpretation of the references to color in this figure legend, the reader is referred to the web version of this article.)

amounts of nano-sized metal particles embedded in 37% S-rich particles. In addition, we devised a conceptual model that describes air pollutant emissions and their transport, clearly indicating the acid cloud or rain formation at Mt. Lu.

Acknowledgments

We are grateful for the help from Xiaolin Ma and Xiaoheng Zhang from Mountain Lu meteorological station. We appreciate Peter Hyde's comments and proofreading. This work was funded by National Natural Science Foundation of China (41105088, 41375126), National Basic Research Program of China (2011CB403401), International Cooperation and Exchanges NSFC-JSPS (41311140168), Fundamental Research Funds of Shandong University (2014QY001-02), and State Key Laboratory of Atmospheric Boundary Physics and Atmospheric Chemistry (LAPC-KF-2013-15).

Appendix A. Supplementary data

Supplementary data related to this article can be found at http://dx.doi.org/10.1016/j.atmosenv.2014.06.003.

References

Adachi, K., Freney, E.J., Buseck, P.R., 2011. Shapes of internally mixed hygroscopic aerosol particles after deliquescence, and their effect on light scattering. Geophys. Res. Lett. 38 (13), L13804 http://dx.doi.org/10.11029/12011GL047540.

AEAERC, 2011. Annual Environment Report of China. AEAERC. http://www.zhb.gov.cn/.

Ahn, K.-H., Kim, S.-M., Jung, H.-J., Lee, M.-J., Eom, H.-J., Maskey, S., Ro, C.-U., 2010. Combined use of optical and electron microscopic techniques for the measurement of hygroscopic property, chemical composition, and morphology of individual aerosol particles. Anal. Chem. 82 (19), 7999–8009.

Bormann, F.H., 1985. Air pollution and forests: an ecosystem perspective. BioScience 35 (7), 434–441.

Brooks, S.D., Wise, M.E., Cushing, M., Tolbert, M.A., 2002. Deliquescence behavior of organic/ammonium sulfate aerosol. Geophys. Res. Lett. 29 (19) http://dx.doi.org/10.1029/2002GL014733.

Cao, Y.-Z., Wang, S., Zhang, G., Luo, J., Lu, S., 2009. Chemical characteristics of wet precipitation at an urban site of Guangzhou, South China. Atmos. Res. 94 (3), 462–469.

Chen, B., Stein, A.F., Maldonado, P.G., Sanchez de la Campa, A.M., Gonzalez-Castanedo, Y., Castell, N., de la Rosa, J.D., 2013. Size distribution and concentrations of heavy metals in atmospheric aerosols originating from industrial emissions as predicted by the HYSPLIT model. Atmos. Environ. 71 (0), 234–244.

Choi, M.Y., Chan, C.K., 2002. The effects of organic species on the hygroscopic behaviors of inorganic aerosols. Environ. Sci. Technol. 36 (11), 2422–2428.

EPA, 2006. Progress Report from the U.S. Environmental Protection Agency. http://www.epa.gov/airmarkets/progress/progress-reports.html.

Freney, E.J., Martin, S.T., Buseck, P.R., 2009. Deliquescence and efflorescence of potassium salts relevant to biomass-burning aerosol particles. Aerosol Sci. Technol. 43 (8), 799–807.

Freney, E.J., Adachi, K., Buseck, P.R., 2010. Internally mixed atmospheric aerosol particles: hygroscopic growth and light scattering. J. Geophys. Res. Atmos. 115 (D19210) http://dx.doi.org/10.1029/2009JD013558.

Galloway, J., Dianwu, Z., Jiling, X., Likens, G.E., 1987. Acid rain: China, United States, and a remote area. Science 236 (4808), 1559–1562.

Gao, X., Xue, L., Wang, X., Wang, T., Yuan, C., Gao, R., Zhou, Y., Nie, W., Zhang, Q., Wang, W., 2012. Aerosol ionic components at Mt. Heng in central southern China: Abundances, size distribution, and impacts of long-range transport. Sci. Total Environ. 433 (0), 498–506.

Giere, R., Blackford, M., Smith, K., 2006. TEM study of PM2.5 emitted from coal and tire combustion in a thermal power station. Environ. Sci. Technol. 40 (20), 6235–6240.

Hao, L., Romakkaniemi, S., Kortelainen, A., Jaatinen, A., Portin, H., Miettinen, P., Komppula, M., Leskinen, A., Virtanen, A., Smith, J.N., Sueper, D., Worsnop, D.R., Lehtinen, K.E.J., Laaksonen, A., 2013. Aerosol chemical composition in cloud events by high resolution time-of-flight aerosol mass spectrometry. Environ. Sci. Technol. 47 (6), 2645–2653.

Harris, E., Sinha, B., van Pinxteren, D., Tilgner, A., Fomba, K.W., Schneider, J., Roth, A., Gnauk, T., Fahlbusch, B., Mertes, S., Lee, T., Collett, J., Foley, S., Borrmann, S., Hoppe, P., Herrmann, H., 2013. Enhanced role of transition metal ion catalysis during in-cloud oxidation of SO_2. Science 340 (6133), 727–730.

Huang, D.-Y., Xu, Y.-G., Peng, P.A., Zhang, H.-H., Lan, J.-B., 2009. Chemical composition and seasonal variation of acid deposition in Guangzhou, South China: comparison with precipitation in other major Chinese cities. Environ. Pollut. 157 (1), 35–41.

Huang, X.-F., Li, X., He, L.-Y., Feng, N., Hu, M., Niu, Y.-W., Zeng, L.-W., 2010. 5-Year study of rainwater chemistry in a coastal mega-city in South China. Atmos. Res. 97 (1–2), 185–193.

Hudson, J.G., 2007. Variability of the relationship between particle size and cloud-nucleating ability. Geophys. Res. Lett. 34 (L08) http://dx.doi.org/10.1029/2006GL028850.

IPCC (Intergovernmental Panel on Climate Change), 2007. Climate Change 2007. In: Solomon, S., Qin, D., Manning, M., Chen, Z., Marquis, M., Averyt, K.B., Tignor, M., Miller, H.L. (Eds.), Climate Change 2007: the Physical Science Basis. Contribution of Working Group I to the Fourth Assessment Report of the Intergovernmental Panel on Climate Change, p. 1056. Cambridge, United Kingdom and New York, 5 NY, USA, 5 (topic 2), New York.

Kahn, R.A., Chen, Y., Nelson, D.L., Leung, F.-Y., Li, Q., Diner, D.J., Logan, J.A., 2008. Wildfire smoke injection heights: two perspectives from space. Geophys. Res. Lett. 35 (4), L04809.

Lack, D.A., Quinn, P.K., Massoli, P., Bates, T.S., Coffman, D., Covert, D.S., Sierau, B., Tucker, S., Baynard, T., Lovejoy, E., Murphy, D.M., Ravishankara, A.R., 2009. Relative humidity dependence of light absorption by mineral dust after long-range atmospheric transport from the Sahara. Geophys. Res. Lett. 36 (24), L24805.

Lei, H.-C., Tanner, P.A., Huang, M.-Y., Shen, Z.-L., Wu, Y.-X., 1997. The acidification process under the cloud in southwest China: observation results and simulation. Atmos. Environ. 31 (6), 851–861.

Li, W., Li, P., Sun, G., Zhou, S., Yuan, Q., Wang, W., 2011a. Cloud residues and interstitial aerosols from non-precipitating clouds over an industrial and urban area in northern China. Atmos. Environ. 45 (15), 2488–2495.

Li, W., Wang, T., Zhou, S., Lee, S., Huang, Y., Gao, Y., Wang, W., 2013a. Microscopic observation of metal-containing particles from Chinese continental outflow observed from a non-industrial site. Environ. Sci. Technol. 47 (16), 9124–9131.

Li, W.J., Shao, L.Y., 2009. Transmission electron microscopy study of aerosol particles from the brown hazes in northern China. J. Geophys. Res. Atmos. 114 (D09)) http://dx.doi.org/10.1029/2008JD011285.

Li, W.J., Shao, L.Y., Buseck, P.R., 2010a. Haze types in Beijing and the influence of agricultural biomass burning. Atmos. Chem. Phys. 10 (17), 8119–8130.

Li, W.J., Zhang, D.Z., Shao, L.Y., Zhou, S.Z., Wang, W.X., 2011b. Individual particle analysis of aerosols collected under haze and non-haze conditions at a high-elevation mountain site in the North China plain. Atmos. Chem. Phys. 11 (22), 11733–11744.

Li, W.J., Wang, Y., Collett, J.L., Chen, J., Zhang, X., Wang, Z., Wang, W., 2013b. Microscopic evaluation of trace metals in cloud droplets in an acid precipitation region. Environ. Sci. Technol. 47 (9), 4172–4180.

Li, Y., Yu, X., Cheng, H., Lin, W., Tang, J., Wang, S., 2010b. Chemical characteristics of precipitation at three Chinese regional background stations from 2006 to 2007. Atmos. Res. 96 (1), 173–183.

Martin, S.T., 2000. Phase transitions of aqueous atmospheric particles. Chem. Rev. 100 (9), 3403–3453.

Marple, V.A., Rubow, K.L., Olson, B.A., 1993. Inertial, gravitational, centrifugal, and thermal collection techniques. In: Willike, K., Baron, P.A. (Eds.), Aerosol Measurement. Van Nostrand Reinhold, New York, pp. 206–233.

Middlebrook, A.M., Bahreini, R., Jimenez, J.L., Canagaratna, M.R., 2011. Evaluation of composition-dependent collection efficiencies for the aerodyne aerosol mass spectrometer using field data. Aerosol Sci. Technol. 46 (3), 258–271.

Peckhaus, A., Grass, S., Treuel, L., Zellner, R., 2012. Deliquescence and efflorescence behavior of ternary inorganic/organic/water aerosol particles. J. Phys. Chem. A 116 (24), 6199–6210.

Posfai, M., Buseck, P.R., 2010. Nature and climate effects of individual tropospheric aerosol particles. Annu. Rev. Earth Planet. Sci. 38 (1), 17–43.

Ramanathan, V., Crutzen, P.J., Kiehl, J.T., Rosenfeld, D., 2001. Atmosphere – aerosols, climate, and the hydrological cycle. Science 294 (5549), 2119–2124.

Ravishankara, A.R., 1997. Heterogeneous and multiphase chemistry in the troposphere. Science 276 (5315), 1058–1065.

Shi, Y., Ge, M., Wang, W., 2012. Hygroscopicity of internally mixed aerosol particles containing benzoic acid and inorganic salts. Atmos. Environ. 60, 9–17.

Sun, M., Wang, Y., Wang, T., Fan, S., Wang, W., Li, P., Guo, J., Li, Y., 2010. Cloud and the corresponding precipitation chemistry in south China: water-soluble components and pollution transport. J. Geophys. Res. Atmos. 115 (D22), D22303.

Tang, J., Xu, X., Ba, J., Wang, S., 2010. Trends of the precipitation acidity over China during 1992–2006. Chin. Sci. Bull. 55 (17), 1800–1807.

Twohy, C.H., Anderson, J.R., 2008. Droplet nuclei in non-precipitating clouds: composition and size matter. Environ. Res. Lett. 3 (4), 045002.

Varutbangkul, V., Brechtel, F.J., Bahreini, R., Ng, N.L., Keywood, M.D., Kroll, J.H., Flagan, R.C., Seinfeld, J.H., Lee, A., Goldstein, A.H., 2006. Hygroscopicity of secondary organic aerosols formed by oxidation of cycloalkenes, monoterpenes, sesquiterpenes, and related compounds. Atmos. Chem. Phys. 6 (9), 2367–2388.

Wang, W., Wang, T., 1995. On the origin and the trend of acid precipitation in China. Water Air Soil. Pollut. 85 (4), 2295–2300.

Whiteaker, J.R., Suess, D.T., Prather, K.A., 2002. Effects of meteorological conditions on aerosol composition and mixing state in Bakersfield, CA. Environ. Sci. Technol. 36 (11), 2345–2353.

Wise, M.E., Biskos, G., Martin, S.T., Russell, L.M., Buseck, P.R., 2005. Phase transitions of single salt particles studied using a transmission electron microscope with an environmental cell. Aerosol Sci. Technol. 39 (9), 849–856.

Wise, M.E., Freney, E.J., Tyree, C.A., Allen, J.O., Martin, S.T., Russell, L.M., Buseck, P.R., 2009. Hygroscopic behavior and liquid-layer composition of aerosol particles generated from natural and artificial seawater. J. Geophys. Res. Atmos. 114, 8.

Xu, J., Bergin, M.H., Yu, X., Liu, G., Zhao, J., Carrico, C.M., Baumann, K., 2002. Measurement of aerosol chemical, physical and radiative properties in the Yangtze delta region of China. Atmos. Environ. 36 (2), 161–173.

Yang, X., 2013. Analysis of Ionic Composition and Sources in Cloud Water at Mount Lu (Master thesis). Shandong University, Jinan, pp. 1–83 (in Chinese).

You, Y., Renbaum-Wolff, L., Carreras-Sospedra, M., Hanna, S.J., Hiranuma, N., Kamal, S., Smith, M.L., Zhang, X., Weber, R.J., Shilling, J.E., Dabdub, D., Martin, S.T., Bertram, A.K., 2012. Images reveal that atmospheric particles can undergo liquid–liquid phase separations. Proc. Natl. Acad. Sci. U. S. A. 109 (33), 13188–13193.

Zhang, Q., Streets, D.G., Carmichael, G.R., He, K.B., Huo, H., Kannari, A., Klimont, Z., Park, I.S., Reddy, S., Fu, J.S., Chen, D., Duan, L., Lei, Y., Wang, L.T., Yao, Z.L., 2009. Asian emissions in 2006 for the NASA INTEX-B mission. Atmos. Chem. Phys. 9 (14), 5131–5153.

Zhang, Q., He, K., Huo, H., 2012. Policy: cleaning China's air. Nature 484 (7393), 161–162.